Quasibound states of quantum dots in single and bilayer graphene

A. Matulis[1,2,*] and F. M. Peeters[1,†]

[1]*Departement Fysica, Universiteit Antwerpen, Groenenborgerlaan 171, B-2020 Antwerpen, Belgium*
[2]*Semiconductor Physics Institute, Goštauto 11, LT-01108 Vilnius, Lithuania*

Dirac fermions interacting with a cylindrically symmetric quantum dot potential created in single and bilayer graphene are not confined but form quasibound states. The broadening of these quasibound states (i.e., the inverse of their lifetimes) decreases (increases) with the orbital momentum of the electron in the case of graphene (bilayer). Quasibound states with energy below (above) the barrier height are dominantly electronlike (holelike). A remarkable decrease of the energy level broadening is predicted for electron energies close to the barrier height, which are a consequence of the total internal reflection of the electronic wave at the dot edge.

I. INTRODUCTION

Quantum dots, or also called "artificial atoms,"[1] are one of the most intensely studied subjects in present day condensed matter physics. Recently, the realization of stable single layer and bilayer carbon crystals (graphene) has aroused considerable interest in the study of their electronic properties.[2–6] These new systems exhibit special excitations which are described by the analogs of the relativistic Dirac equation.[7] One of the most impressive effects is the so-called Klein paradox according to which electrons can cross large electric barriers with unity probability.[8,9] As a consequence, the control of the electron behavior by means of electrical potentials and structures becomes a very challenging task and the creation of quantum dots in such materials is not obvious.

It follows from the Klein effect straightforwardly that the electron will escape from any potential minimum and that there are no bound states in an electrically defined quantum dot (except in a gated bilayer[10] or in a graphene ribbon[11] when the band degeneracy is lifted by some additional means). However, the polar diagrams presented in Ref. 8 indicate that in single and bilayer graphene, the electron penetration into a potential barrier is strongly reduced if this electron propagates at some angles with respect to the barrier. From this observation, we may expect that there might be long living *quasibound states* in such quantum dots for specific orbital momenta of the electrons. These states may be probed in experiments, say by tunneling currents directed perpendicular to the dot using, e.g. scanning tunneling microscopy (STM), or in the near field infrared absorption, as narrow peaks in the local density of states.

In this work, we impose a circularly symmetric quantum dot potential as created, e.g., by the split gate technique in single layer and bilayer graphene, and discuss the conditions under which the quasibound states can appear. Such a problem was recently discussed in Ref. 12 where the semiclassical approach was applied to the problem of electron motion in a parabolic quantum dot and the imaginary part of the energy eigenvalues (i.e., the lifetime of those states) was calculated. The possibility to confine the electrons by an external potential in a small region of a graphene strip was also discussed in Ref. 13. Our approach is essentially different

from Ref. 12 in two ways: (1) we define the quasibound states through the averaged local density of states, and (2) we study a quantum dot with a step profile instead of a parabolic dot where the potential tends to infinity at large distances. We found that the width of those quasibound states (i.e., the inverse of their lifetime) (1) has the opposite dependence on the angular quantum number for a single and a bilayer graphene and (2) that it becomes extremely small for energies near the potential barrier height.

The paper is organized as follows. In Sec. II, we formulate the problem of a quantum dot in graphene. Its solution is given in Sec. III, and in Sec. IV, the averaged local density of states is considered. The results for a single graphene layer are presented in Sec. V. In Sec. VI, the same quantum dot problem is formulated for a bilayer of graphene, and its solution and results are given in Sec. VII. Our conclusions are formulated in Sec. VIII.

II. QUANTUM DOT IN GRAPHENE

From the point of view of its electronic properties, graphene can be considered as a two-dimensional zero-gap semiconductor with its low-energy quasiparticles (electrons and holes) described by the Dirac-like Hamiltonian,[8]

$$H_0 = v_F \boldsymbol{\sigma} \mathbf{p}, \tag{1}$$

where $v_F \approx 10^6$ m s^{-1} is the Fermi velocity and $\boldsymbol{\sigma} = (\sigma_x, \sigma_y)$ are the Pauli matrices. We assume that the total Hamiltonian consists of the above Hamiltonian of free particles in addition to the cylindrically symmetric electric confinement potential,

$$V(\mathbf{r}) = V\Theta(r - a) = \begin{cases} 0, & 0 \leq r < a \\ V, & a \leq r < \infty. \end{cases} \tag{2}$$

Such potential can be created by means of a patterned gate electrode when the edge smearing is much less than the characteristic Fermi wavelength of the electrons and, in turn, much larger than the graphene lattice constant.

As the electric potential cannot confine the electrons in a finite region of the graphene plane, there are no bound states. Consequently, the electron will have a continuous spectrum, and electron states in the quantum dot have to be described

as decaying quasibound states. Nevertheless, we shall consider this problem as a stationary one by artificially confining the electron within a large sample. We shall solve the stationary equation,

$$\{H - E\}\Psi(\mathbf{r}) = 0, \quad H = H_0 + V(\mathbf{r}), \tag{3}$$

in a finite graphene circle of radius R. In this case, the energy spectrum consists of discrete levels separated by intervals which go to zero as R^{-1} when R tends to infinity. The presence of quasibound states in the quantum dot can show up as peaks in the averaged electron density in the dot. They can be revealed experimentally as peaks in the tunneling current through this dot in, e.g., a STM experiment.

III. SOLUTION OF EIGENVALUE PROBLEM

For the sake of convenience, we introduce dimensionless variables, measuring the distance in the units of the quantum dot radius a and energies in $\hbar v_F / a$ units. For instance, for a dot with radius $a = 0.1$ μm, the above energy unit is 6 meV. It enables us to write the Hamiltonian as

$$H = \begin{pmatrix} V\Theta(r-1) & -i(\partial/\partial x - i\partial/\partial y) \\ -i(\partial/\partial x + i\partial/\partial y) & V\Theta(r-1) \end{pmatrix}. \tag{4}$$

Lets write the two component wave function as

$$\Psi(\mathbf{r}) = \begin{pmatrix} A(\mathbf{r}) \\ B(\mathbf{r}) \end{pmatrix}, \tag{5}$$

and taking into account the cylindrical symmetry of the problem, where we use

$$\frac{\partial}{\partial x} - i\frac{\partial}{\partial y} = e^{-i\varphi}\left(\frac{\partial}{\partial r} - \frac{i}{r}\frac{\partial}{\partial \varphi}\right), \tag{6}$$

the eigenfunction problem (3) can be written as two coupled differential equations for the wave function components,

$$(V - E)A = ie^{-i\varphi}\left(\frac{\partial}{\partial r} - \frac{i}{r}\frac{\partial}{\partial \varphi}\right)B, \tag{7a}$$

$$(V - E)B = ie^{i\varphi}\left(\frac{\partial}{\partial r} + \frac{i}{r}\frac{\partial}{\partial \varphi}\right)A. \tag{7b}$$

These equations can be further simplified by using the circle symmetry of our problem which allows us to assume the following angular dependence of the wave function components:

$$\begin{pmatrix} A(\mathbf{r}) \\ B(\mathbf{r}) \end{pmatrix} = e^{im\varphi}\begin{pmatrix} a(r) \\ ie^{i\varphi}b(r) \end{pmatrix}, \tag{8}$$

where the integer m stands for the eigenstate angular momentum. This assumption converts Eq. (7) into the following set of coupled ordinary radial differential equations:

$$(V - E)a = -\left(\frac{d}{dr} + \frac{m+1}{r}\right)b, \tag{9a}$$

$$(V - E)b = \left(\frac{d}{dr} - \frac{m}{r}\right)a. \tag{9b}$$

These two equations have to be solved in the inner ($r < 1$) and outer ($1 < r < R$) regions of the dot ensuring the continuity of both wave function components (a and b) at the quantum dot edge $r = 1$. Moreover, the proper boundary condition has to be satisfied at the sample edge ($r = R$). Although the exact boundary condition depends on which sublattice atoms are located at the sample edge, we restrict our consideration to the simple equation

$$a(R) = 0, \tag{10}$$

as the average local density of states which we are looking for is not sensitive to the microscopic details of the sample edge.

Now, inserting b from Eq. (9b) into Eq. (9a), we arrive at the second order ordinary differential equation,

$$\left(\frac{d^2}{dr^2} + \frac{1}{r}\frac{d}{dr} - \frac{m^2}{r^2}\right)a = -(V - E)^2 a, \tag{11}$$

which actually coincides with the Bessel function equation. The other wave function component can be easily obtained from Eq. (9b). Thus, the solution inside the dot [where $V(r) = 0$] in the case of positive energy $E > 0$ reads

$$a = FJ_m(Er), \tag{12a}$$

$$b = FJ_{m+1}(Er). \tag{12b}$$

Note that we did not include the Bessel function of second order $Y_m(Er)$ into our solution, as it is singular at $r = 0$. Outside the dot ($1 \leq r < R$), the solution is

$$a = PJ_m(\kappa r) + QY_m(\kappa r), \tag{13a}$$

$$b = \mp\{PJ_{m+1}(\kappa r) + QY_{m+1}(\kappa r)\}, \tag{13b}$$

where

$$\kappa = |E - V|, \tag{14}$$

and the sign in the right hand side of the b expression coincides with the sign of $(E - V)$.

Satisfying the boundary conditions, we obtain the following set of algebraic equations for the coefficients (F, P, Q):

$$FJ_m(E) = PJ_m(\kappa) + QY_m(\kappa), \tag{15a}$$

$$FJ_{m+1}(E) = \mp\{PJ_{m+1}(\kappa) + QY_{m+1}(\kappa)\}, \tag{15b}$$

$$PJ_m(\kappa R) + QY_m(\kappa R) = 0. \tag{15c}$$

As we are interested in the limiting case $R \to \infty$, we replace the Bessel functions in Eq. (15c) by their asymptotic expressions, which results into

$$P \cos\left(\kappa R - \frac{\pi m}{2} - \frac{\pi}{4} \right) + Q \sin\left(\kappa R - \frac{\pi m}{2} - \frac{\pi}{4} \right) = 0.$$

$$(16)$$

Up to a normalization factor, the solution of this equation can be chosen as

$$P = \sin\left(\kappa R - \frac{\pi m}{2} - \frac{\pi}{4} \right), \qquad (17a)$$

$$Q = -\cos\left(\kappa R - \frac{\pi m}{2} - \frac{\pi}{4} \right). \qquad (17b)$$

IV. LOCAL DENSITY OF STATES

Inserting the obtained solution for the P and Q coefficients into Eqs. (15a) and (15b), we arrive at the equation for the eigenvalues. It follows from Eq. (17) that these eigenvalues are separated by

$$\Delta E = \Delta \kappa = \frac{\pi}{R}. \qquad (18)$$

These dense discrete energy levels are a consequence of the finite size of our sample and are not of interest to us. Therefore, we choose another procedure and solve the two equations [Eqs. (15a) and (15b)] together with the condition

$$P^2 + Q^2 = 1, \qquad (19)$$

which is clearly satisfied as it follows from Eq. (17). This procedure enables us to obtain the local density of states from which we can derive the quasibound states. The procedure is as follows.

First, we calculate the normalization factor N of the wave function. In the limiting case $R \rightarrow \infty$, it can be done by just using the asymptotic wave function expression, namely,

$$1 = 2(2\pi N^2) \int_0^R r dr \left(\frac{2}{\pi \kappa r} \right) \left\{ P \cos\left(\kappa r - \frac{\pi m}{2} - \frac{\pi}{4} \right) \right.$$

$$\left. + Q \sin\left(\kappa r - \frac{\pi m}{2} - \frac{\pi}{4} \right) \right\}^2 = \frac{4N^2 R}{\kappa}(P^2 + Q^2). \quad (20)$$

The additional factor 2 appears because both wave function components have to be taken into account. Using Eq. (19), we find

$$N = \sqrt{\frac{\kappa}{4R}}. \qquad (21)$$

Next, we point out that any physical property of the quantum dot, say like the tunneling current through the dot or the absorption of the infrared radiation in near field spectroscopy, can be expressed as a summation of some matrix elements over the above dense quantum states. The matrix elements are integrals over the quantum dot area, namely,
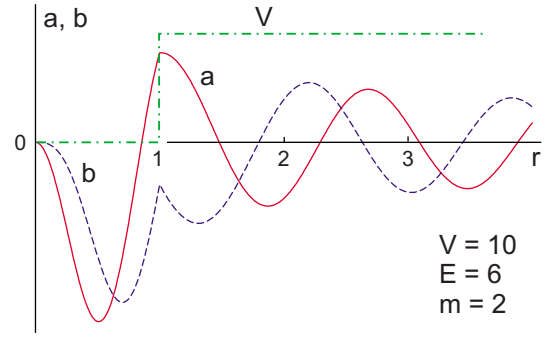

FIG. 1. (Color online) Profile of the confinement potential (dot-dash curve) and the two wave function components: a, solid curve and b, dashed curve. Barrier height $V=10$, energy $E=6$, and orbital momentum $m=2$.

$$M = 2\pi N^2 F^2 \int_0^1 r dr f(r) \{ J_m^2(Er) + J_{m+1}^2(Er) \}, \qquad (22)$$

where the function $f(r)$ characterizes the interaction of the quantum dot with the measuring probe. This function was recently measured in the case of an atomic force microscopy tip interacting with a "normal" two-dimensional electron gas.[14] Thus, replacing the summation over the discrete levels by an integration, in accordance with Eq. (18),

$$\sum_n M \approx \frac{R}{\pi} \int dE M \sim 2R \int dE N^2 F^2 = \int dE \frac{\kappa F^2}{2}, \quad (23)$$

we see that within the accuracy of the experimental form factor [the integral in the right hand side of Eq. (22)], the quantity

$$\rho(E) = \tfrac{1}{2} |E - V| F^2 \qquad (24)$$

acts as a local density of states in the quantum dot area.

Here, we have to point out the role of the integration with the form factor $f(r)$ in Eq. (22) which mainly depends on the effective width of the tip used in the STM experiment. The local density of states [Eq. (24)] can be measured in the case when this width is of the same order as the quantum dot diameter. In the case of a narrow tip, the value of the squared wave function in the dot is measured instead, while in the opposite case of a wide tip, the peaks of the quasibound states are washed out.

It is remarkable that the obtained local density of states consists of two factors. One of them $|E - V|$ is just the density of states of the free hole (or electron) in the barrier region, while the other one F^2 is its modulation caused by the quantum dot itself.

V. RESULTS FOR QUANTUM DOT IN GRAPHENE

We solved Eqs. (15a), (15b), and (19) numerically from which we obtained the coefficients and the local density of states [Eq. (24)]. A typical example for the two components of the wave function together with the confinement potential profile is shown in Fig. 1.

As the energy is lower than the potential height, we see that the two wave function components have a different
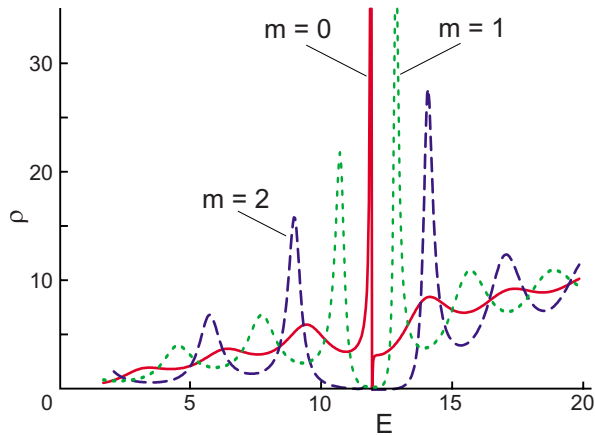
FIG. 2. (Color online) Local density of states as a function of the energy in case of barrier height $V=12$ for the orbital momenta $m=0$ (solid curve), $m=1$ (dotted curve), and $m=2$ (dashed curve).

phase indicating the electronic type character of the wave function inside the dot and the hole type character outside it. The large value of the wave function components inside the dot shows that this eigenfunction is a quasibound state.

Typical local density of states is shown in Fig. 2.

It exhibits peaks which can be associated with the quasibound states of the dot. The increasing background can also be revealed, which is a consequence of the above mentioned factor $|E-V|$ in Eq. (24) corresponding to the density of states of a free electron or hole in the barrier region. The three curves in Fig. 2 correspond to the following orbital momenta of electron $m=0,1,2$. We observe the general tendency that the larger the orbital momentum, the narrower the peaks are. Notice the very narrow peak when the energy is close to the barrier height (see the curve for $m=0$). This tendency is even better seen in Fig. 3 where the positions and broadenings of the peaks are shown.

We fitted the peaks in the density of states by the Lorentzian functions $a_n\gamma_n/\{(E-E_n)^2+\gamma_n^2\}$ defining three parameters for any of them: the position E_n, its broadening γ_n, and the amplitude a_n. Graphically, these parameters are shown in Fig. 3 for two orbital momentum m values as a function of the barrier height V.

The positions E_n of the quasibound levels are shown by the solid curves, while the shaded areas between two $E_n \pm \gamma_n$ curves indicate the broadening of them. As expected, in the case $m=0$ [Fig. 3(a)], the levels are rather broad. Actually, they can hardly be identified as quasibound levels and they rather correspond to weak oscillations in the local density of states of the continuous spectrum (see the solid curve in Fig. 2).

In the case of $m=2$, we see [Fig. 3(b)] a quite different picture. The levels are narrow and indicate the presence of long living quasibound states. It is interesting to see that the quasibound states are seen above as well as below the barrier; the latter is indicated by the slant solid line. Actually, this is the consequence of the equivalence of the Dirac electrons and holes in the barrier region.

As was already mentioned in Fig. 3, we see one more important peculiarity of the local density of states for a quantum dot in graphene. This is the extremely narrow width of
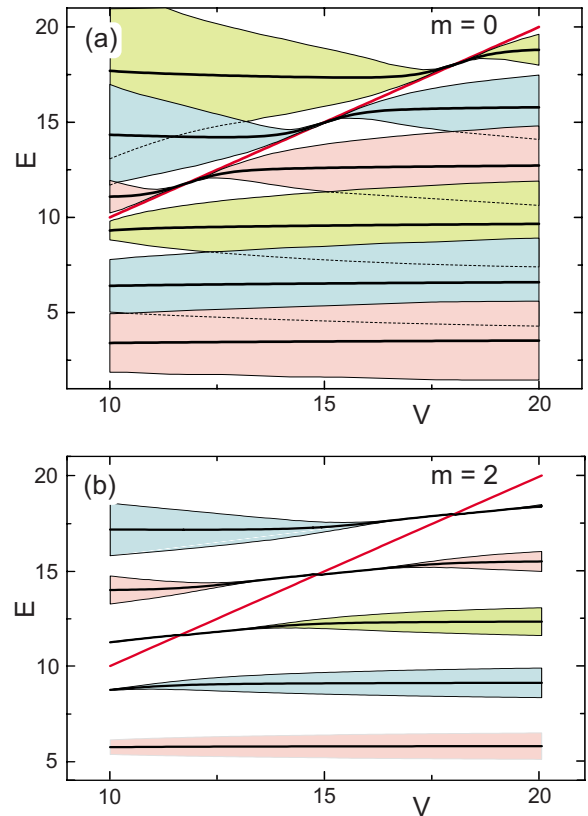

FIG. 3. (Color online) Quasibound states for a quantum dot in graphene: orbital momenta (a) $m=0$, (b) $m=2$. The energies of these states are given by the black curves and its width (i.e., the inverse of the lifetime) by the colored region. The straight slanted line corresponds to $E=V$.

the states in the vicinity of the top of the barrier. This is not an accidental phenomena, but the consequence of the important fact that it is rather difficult for the Dirac electrons to penetrate the barrier when its energy is close to the barrier height. This property follows straightforwardly from the electron penetration through the barrier problem solved in Refs. 8 and 9; no attention was payed to this limiting case. The matter is that the angle φ (with respect to the perpendicular to the barrier, see the inset of Fig. 4) of the incident electron and the angle ψ of the refracted electron have to satisfy the equation

$$E \sin \varphi = (V - E)\sin \psi, \qquad (25)$$

which is the equivalent of Snell's law in optics.[15] For the case when the electron energy is close to the barrier height,

$$E = V - \Delta, \quad |\Delta| \ll V, \qquad (26)$$

the electron wave goes from the material with large refraction index into the material with small refraction index. In this case, the well-known phenomena of total internal reflection take place. It means that there is a critical incident angle

$$\varphi_0 = |\Delta|/V, \qquad (27)$$

such that electrons with larger incident angles ($|\varphi| > \varphi_0$) are totally reflected from the barrier (see the inset of Fig. 4,
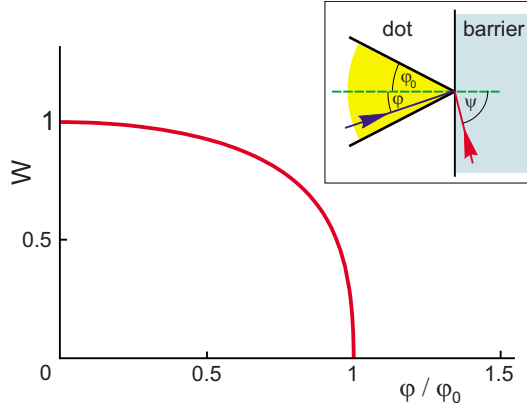
FIG. 4. (Color online) Tunneling probability dependence on the incident angle of the electron beam in the case of small deviation of the electron energy from the barrier height. Inset: definition of the critical angle φ_0.

where the angles at which the electron penetrates the barrier are shown by the shadowed sector). The electron current (which is proportional to the tunneling probability) in the barrier perpendicular to the barrier edge direction can be expressed as follows:

$$W = \frac{2\sqrt{\varphi_0^2 - \varphi^2}\,\Theta(\varphi_0 - \varphi)}{\varphi_0 + \sqrt{\varphi_0^2 - \varphi^2}}, \tag{28}$$

and it is shown in Fig. 4.

So, when the electron energy is close to the barrier height, there is only a very small region of the incident angles at which the electron can penetrate the barrier. It means that for these electrons, the electrical barrier acts almost as a confining potential. This explains why in this energy region very narrow quasibound levels appear even for zero orbital momentum.

VI. QUANTUM DOT IN BILAYER GRAPHENE

It is instructive to consider the same quantum dot problem for bilayer graphene. There are similarities and differences between the two graphene systems.[16] Both systems have gapless electron and hole spectra but are described by different Dirac type Hamiltonians.

Following Ref. [8], we use the two component wave function approximation for the bilayer which is described by the following Hamiltonian:

$$H_0 = \frac{1}{2}\begin{pmatrix} 0 & (\partial/\partial x - i\partial/\partial y)^2 \\ (\partial/\partial x + i\partial/\partial y)^2 & 0 \end{pmatrix}, \tag{29}$$

where the distances are measured as before in units of the quantum dot radius a and the energies are measured in $\hbar^2/m^*a^2$ units. For example, for a dot with radius $a = 0.1\ \mu m$ and the effective mass[16] $m^* = 0.038 m_e$, the above energy unit is 0.2 meV.

Assuming expressions for the wave function analogous to those for graphene [Eq. (5)], we obtain the following set of equations for the wave function components:

$$(E-V)A = \frac{1}{2}\left(\frac{\partial}{\partial x} - i\frac{\partial}{\partial y}\right)^2 B, \tag{30a}$$

$$(E-V)B = \frac{1}{2}\left(\frac{\partial}{\partial x} + i\frac{\partial}{\partial y}\right)^2 A. \tag{30b}$$

The components A and B have to satisfy the continuity condition together with the continuity of their first radial derivatives at the dot edge.

In the dot and as well outside it, these two equations can be transformed into a single equation for any wave function component,

$$\left\{\frac{1}{2}\nabla^4 - (E-V)^2\right\}A = \left\{\frac{1}{2}\nabla^2 + (E-V)\right\}\left\{\frac{1}{2}\nabla^2 - (E-V)\right\}A$$
$$= 0. \tag{31}$$

Using the axial symmetry and assuming the following angular dependence,

$$A(\mathbf{r}) = e^{im\varphi}a(r), \tag{32}$$

this component has to satisfy any of the following radial equations:

$$\left\{\frac{d^2}{dr^2} + \frac{1}{r}\frac{d}{dr} + \left[\pm(E-V) - \frac{m^2}{r^2}\right]\right\}a = 0. \tag{33}$$

It is evident that they are the equations for the Bessel (plus sign) and modified Bessel (minus sign) functions. Inside the quantum dot ($r \leq 1$), the solution is

$$a = FJ_m(kr) + GI_m(kr), \tag{34}$$

where $k = \sqrt{2E}$. Two other solutions (Y_m and K_m) are not included because of their singularity at the origin $r=0$. Similarly, using Eq. (30b), we obtain for the other component of the wave function,

$$B(\mathbf{r}) = e^{i(m+2)\varphi}b(r), \tag{35a}$$

$$b = FJ_{m+2}(kr) + GI_{m+2}(kr). \tag{35b}$$

Outside the quantum dot, the wave function components are given by

$$A = PJ_m(\kappa r) + QY_m(\kappa r) + SK_m(\kappa r), \tag{36a}$$

$$B = \mp\{PJ_{m+2}(\kappa r) + QY_{m+2}(\kappa r) + SK_{m+2}(\kappa r)\}, \tag{36b}$$

where $\kappa = \sqrt{2|E-V|}$ and the sign of the B component coincides with the sign of the expression $(E-V)$. We do not include the functions I_n and I_{m+2} into the above expressions, as these functions are responsible only for satisfying the boundary condition at the sample edge $r=R$ and are therefore not relevant in the limit $R \to \infty$.

In analogy to our approach for graphene, we equate both wave function components and their derivatives at the quantum dot edge ($r=1$), and together with Eq. (19), we obtain a set of five algebraic equations for the five parameters F, G, P, Q, and S.

We point out that the functions $I_m(kr)$ and $K_m(\kappa r)$ together with the analogs for orbital momentum $m+2$ are essential
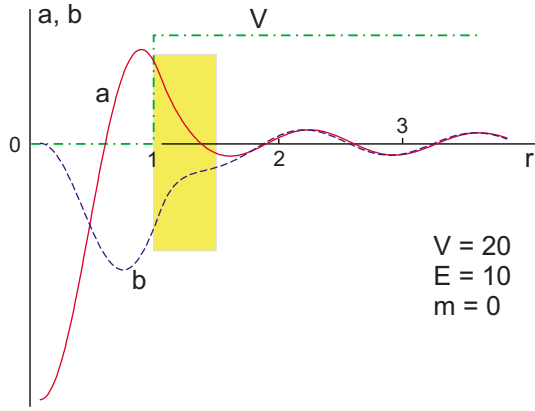
FIG. 5. (Color online) Wave function components in bilayer: $V=20$, $E=10$, $m=0$; solid curve, component a; dashed curve, component b; the dash-dotted curve is the potential profile of the dot.

only in the region close to the dot edge, where they ensure the continuity of the derivatives of the wave function components. The main contribution to the local density of states is determined by the functions $J_m(kr)$ and $J_{m+2}(kr)$. Following the procedure presented in Sec. IV, we obtain the following expression for the quantum dot local density of states in a bilayer:

$$\rho(E) = \tfrac{1}{2}F^2. \qquad (37)$$

Note that it differs from the analogous expression for the case of graphene by the factor depending on the electron energy in the barrier, what is caused by the constant free electron (hole) density of states for the case of parabolic energy band in the barrier region.

VII. RESULTS FOR THE QUANTUM DOT IN BILAYER GRAPHENE

Solving numerically the set of equations for the coefficients, introduced in the previous section, we calculated the wave functions and the local density of states. An example of the wave function is shown in Fig. 5.

Comparing it with the wave function for the dot in graphene, we notice several differences. The derivative of the wave function in a bilayer is continuous at the dot edge, while in graphene, the wave function components exhibit kinks. That is the reason why in a bilayer there is an intermediate region of exponential behavior (see the shadowed rectangle in Fig. 5) where the electron type function changes itself into the hole type one.

The local density of states of the quantum dot states is shown in Fig. 6 for the case of two orbital momenta ($m=0$ and $m=2$). These pictures also differ essentially from those for graphene shown in Fig. 3.

First, we see that the quasibound states with energy lower than the barrier height in a bilayer are much narrower as compared with these in graphene. The main reason of this difference is as follows. Although single layer graphene and bilayer graphene are both gapless materials, the physical nature of their bands is quite different. In graphene, the electron
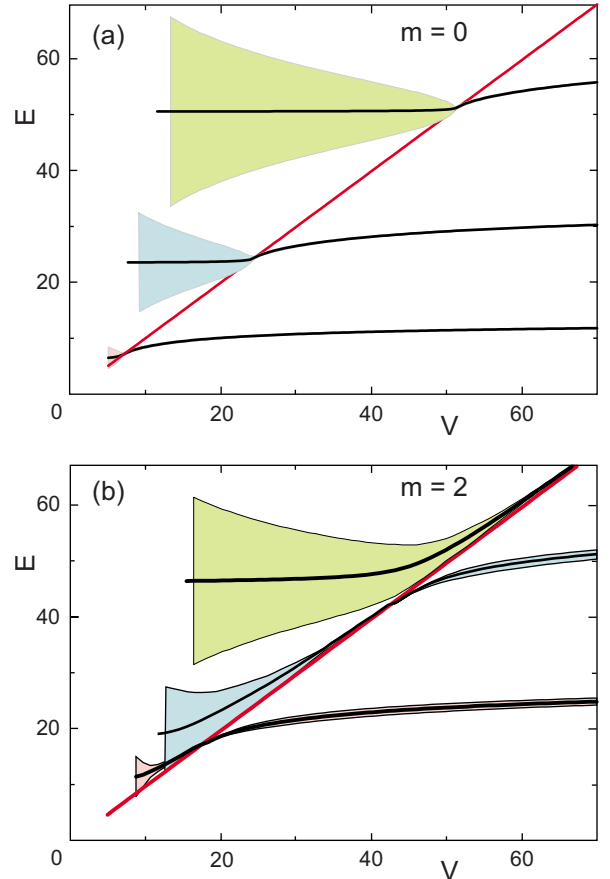

FIG. 6. (Color online) Quasibound states for quantum dot in bilayer: orbital momenta (a) $m=0$, (b) $m=2$. The energies of these states are given by the black curves and its width (i.e., the inverse of the lifetime) by the shadowed regions. The straight slanted line corresponds to $E=V$.

and hole parts of the bands are the natural prolongation of each other. Electrons and holes are like different expressions of the same Dirac quasiparticle. While in bilayer graphene, these two contiguous electron and hole bands are much more independent from one another, and it reminds one to the accidental touching of their extremum points.

This can be more clearly demonstrated by rewriting the component equations [Eq. (30)] in the case of perpendicular incidence of the electron to the barrier,

$$(E - V)A = \frac{1}{2}\frac{d^2}{dx^2}B, \qquad (38a)$$

$$(E - V)B = \frac{1}{2}\frac{d^2}{dx^2}A. \qquad (38b)$$

Adding and subtracting these equations, we obtain the set of uncoupled equations for the hole $A+B$ and electron $A-B$ type wave functions. Consequently, in the case of perpendicular incidence, the electron in a bilayer can be confined in the dot by the electrical potential, and thus, we obtain stationary states. In the case of slanted incidence, when the electron momentum component $k_\parallel$ along the barrier is not zero, the equations can no longer be decoupled. In this case,

this longitudinal momentum (or the orbital momentum of the electron) serves as a coupling constant between the electron and the hole. Consequently, the larger the angular momentum, the larger the probability for the electron to convert itself into a hole, or the more dominant the Klein effect is, and thus the more smeared the quasibound level is. This is actually seen in Fig. 6 which shows that the quasibound states for $m=0$ are narrower as compared to the $m=2$ states. By the way, this difficult penetration of the electron into the barrier is indicated by the intermediate exponential region in the wave function coordinate dependence, as shown by the shadowed area in Fig. 5.

This simple physical picture explains one more interesting property of the above local dot density of states. In Fig. 3, we see that in graphene, there is some symmetry between the quasibound states below the top of the barrier (red solid slanted line) and above it. While in bilayer graphene, as seen in Fig. 6, such symmetry is absent and the states above and below the top are quite different. The states above the top of the barrier, are much more smeared. This is caused by the fact that above the barrier, the nature of the wave function is the same in both regions (in the dot and outside it), and there is no need for the electron to transform itself into a hole, and consequently, the probability to escape the dot is larger than in the opposite case when the energy is smaller than the top of the barrier.

VIII. SUMMARY AND CONCLUSIONS

Using the two wave function component approximation, we calculated the local density of states in an electrically defined circle symmetric quantum dot in single layer and bilayer graphene. It was shown that in bilayer graphene, rather narrow quasibound states appear when the energy is smaller than the barrier height. The broadening of the states in bilayer graphene increases as the orbital momentum becomes larger which is opposite to the case of graphene.

In contrast, in graphene, narrow quasibound states are predicted with increasing orbital momentum. This different behavior of the quasibound states in graphene and bilayer graphene is explained by the different physical nature of the touching electron and hole energy bands.

Weakly broadened quasibound states are predicted in both graphene and bilayer graphene in the region where the electron energy is close to the top of the barrier. This phenomena can be understood from an analog of the optical effect of total internal reflection which an electron wave suffers in the above mentioned region of energies.

We also notice the different symmetry of the states above and below the top of the barrier in single layer graphene and bilayer graphene, caused by the different way of electron conversion into a hole in both systems.

*amatulis@takas.lt

†francois.peeters@ua.ac.be

[1] T. Chakraborty, *Quantum Dots* (Elsevier, Amsterdam, 1999).

[2] Y. Zheng and T. Ando, Phys. Rev. B **65**, 245420 (2002).

[3] K. S. Novoselov, A. K. Geim, S. V. Morozov, D. Jiang, Y. Zhang, S. V. Dubonos, I. V. Grigorieva, and A. A. Firsov, Science **306**, 666 (2004).

[4] K. S. Novoselov, A. K. Geim, S. V. Morozov, D. Jiang, M. I. Katsnelson, I. V. Grigorieva, S. V. Dubonos, and A. A. Firsov, Nature (London) **438**, 197 (2005).

[5] Y. Zheng, Y. W. Tan, H. L. Stormer, and P. Kim, Nature (London) **438**, 201 (2005).

[6] V. P. Gusynin and S. G. Sharapov, Phys. Rev. Lett. **95**, 146801 (2005).

[7] K. S. Novoselov, E. McCann, S. V. Morozov, V. I. Fal'ko, M. I. Katsnelson, U. Zeitler, D. Jiang, F. Schedin, and A. K. Geim, Nat. Phys. **2**, 177 (2006).

[8] M. I. Katsnelson, K. S. Novoselov, and A. K. Geim, Nat. Phys. **2**, 620 (2006).

[9] J. Milton Pereira, Jr., P. Vasilopoulos, and F. M. Peeters, Appl. Phys. Lett. **90**, 132122 (2007).

[10] J. Milton Pereira, Jr., P. Vasilopoulos, and F. M. Peeters, Nano Lett. **7**, 946 (2007).

[11] B. Trauzettel, D. V. Bulaev, D. Loss, and G. Burkard, Nat. Phys. **3**, 192 (2007).

[12] Hong-Yi Chen, Vadim Apalkov, and Tapash Chakraborty, Phys. Rev. Lett. **98**, 186803 (2007).

[13] P. G. Silvestrov and K. B. Efetov, Phys. Rev. Lett. **98**, 016802 (2007).

[14] A. E. Gildemeister, T. Ihn, M. Sigrist, K. Ensslin, D. C. Driscoll, and A. C. Gossard, Phys. Rev. B **75**, 195338 (2007).

[15] V. V. Cheianov, V. Fal'ko, and B. Altshuler, Science **315**, 1252 (2007).

[16] B. Partoens and F. M. Peeters, Phys. Rev. B **74**, 075404 (2006).